Dimensions of the Narrow Portion of a Recombinant NMDA Receptor Channel

A. Villarroel, N. Burnashev, and B. Sakmann
Max-Planck-Institut für medizinische Forschung, Abteilung Zellphysiologie, D-69120 Heidelberg, Germany

ABSTRACT Glutamate-activated single-channel and ensemble currents were recorded from *Xenopus laevis* oocytes and HEK 293 cells expressing a recombinant NMDA receptor, assembled from NR1 and NR2A subunits. Cesium was the main charge carrier, and organic cations were used to determine the presence of vestibules of this channel and to estimate its pore diameter. The large organic cations tris-(hydroxymethyl)-aminomethane (Tris), N-methyl-glucamine (NMG), arginine (Arg), choline, and tetramethylammonium (TMA), when added in millimolar concentrations to the extracellular or cytoplasmic side, produced a voltage-dependent blockade of single-channel Cs^+ currents. These molecules behaved as impermeant ions that only partially traverse the channel from either side. The smaller cations trimethylammonium (TriMA) and dimethylammonium (DMA) produced a small and nearly voltage-independent reduction in current amplitude, suggesting that they are permeant. In biionic experiments with Cs^+ as the reference ion, the large blocking cations NMG, Arg, Tris, TMA, choline, hexamethonium (Hme), triethylammonium (TriEA), and tetraethylammonium (TEA) showed no measurable permeability. TriMA and smaller ammonium derivatives were permeant. Both the permeability and single-channel conductance of organic cations, relative to Cs^+, decreased as the ion size increased. The results suggest that the NMDA receptor has extracellular and cytoplasmic mouths that can accommodate large cations up to 7.3 Å in mean diameter. The narrow portion of the pore is estimated to have a mean diameter of 5.5 Å.

INTRODUCTION

The N-methyl-D-aspartic acid receptor (NMDAR) forms a cation-selective channel at excitatory synapses of the mammalian central nervous system. It is distinguished from other glutamate receptors by its distinct pharmacological and functional properties (Watkins, 1981; Mayer and Westbrook, 1984; Cull-Candy et al., 1988). A ubiquitously expressed NR1 subunit (Moriyoshi et al., 1991) forms functional channels when coexpressed with a subunit from the NR2 subunit family, suggesting that native NMDARs are composed of the NR1 subunit combined with one or more members of the NR2 subunit family (Monyer et al., 1992, Kutsuwada et al., 1992; Ishii et al., 1993). Channels formed by NR1 and NR2A subunits expressed in different host cells have similar properties (Stern et al., 1994) and offer the possibility to study the ion conduction pathway of a NMDAR channel of defined molecular composition.

The gross structure of the pore of ion channels can be explored using organic cations of different size. Compounds such as tris-(hydroxymethyl)-aminomethane (Tris), tetraethylammonium (TEA), and other ammonium derivatives penetrate into the conduction pathway of cation-selective channels and produce a voltage-dependent block (Armstrong, 1975; Hille, 1992). The voltage dependence of the blockade and the diameter of a blocking ion may give estimates of the dimension and location of a putative wider funnel that forms the entry to the narrow portion of the channel (Miller, 1982; Coronado and Miller, 1982; Villarroel et al., 1988). The narrow region of the pore can also be probed with organic ions. By using a simple hydrodynamic model, the cross-sectional area of the narrow part of the pore can be estimated (Dwyer et al., 1980; Bormann et al., 1987; Yang, 1990).

Compared with other ligand-gated channels, relatively little is known about the dimensions of the ion conduction pathway of NMDAR channels. It has been suggested that in native membranes its minimal diameter is slightly less than that of kainate-activated glutamate receptor channels (Vyklicky et al., 1988) and is similar to that of nicotinic AChR channels (Wright et al., 1991). Several experimental difficulties may arise, however, when studying native NMDAR channels. Because these channels are highly permeable to Ca^{2+}, any permeability and conductance measurements made in the presence of physiological $[Ca^{2+}]$ have to be corrected accordingly. In addition, native NMDAR channels are heterogeneous in their conductance (Cull-Candy and Usowicz, 1987; Jahr and Stevens, 1987) and presumably in their subunit composition (Monyer et al., 1994).

We have used organic cations to explore the dimension of the narrow portion of the recombinant NMDAR channel formed by NR1 and NR2A subunits. To circumvent the potential difficulties due to the high Ca^{2+} permeability of this receptor, we have made permeability measurements in the presence and absence of Ca^{2+}. Some of the present results have been presented in preliminary form (Villarroel, 1993).

Received for publication 17 June 1994 and in final form 13 December 1994.

Address reprint requests to Dr. Alfredo Villarroel, Max-Planck-Institut für medizinische Forschung, Abteilung Zellphysiologie, Jahnstr. 29, D-69120 Heidelberg, Germany. Tel.: 06221-486-460; Fax: 06221-486-459; E-mail: alfredo@sunny.mpimf-heidelberg.mpg.de.

0006-3495/95/03/866/10 $2.00

MATERIALS AND METHODS

Materials

Methylammonium (MA), dimethylammonium (DMA), trimethylammonium (TriMA), triethylammonium (TriEA), tetramethylammonium (TMA), arginine (Arg), N-methyl-glucamine (NMG), Tris, choline, TEA,

L-glutamic acid, hexamethonium (Hme), and glycine were obtained from Sigma Chemical Co. (St. Louis, MO). Glycine and glutamate were kept frozen in 10 mM stock solutions.

Heterologous expression of NMDAR channels

Xenopus oocytes were injected with mRNAs encoding the NR1 and NR2A subunits of the NMDAR in the molar proportion 1:2 as described previously (Methfessel et al., 1986). Three days after injection experiments were made on inside-out or outside-out oocyte patches. Human embryonic kidney cells (HEK 293 cell line, referred to as HEK cells in the text) were transfected with cDNAs encoding the NR1 and NR2A subunits (Chen and Okayama, 1987; Monyer et al., 1992) and whole-cell currents were measured 2 days after transfection (Burnashev et al., 1992).

Channel conductance and permeability

Single-channel currents were recorded (at 18°C) from inside-out oocyte membrane patches (Hamill et al., 1981; Methfessel et al., 1986) with pipettes of 5 MΩ wt resistance when filled with 100 mM CsCl, 10 mM HEPES, and 10 mM EGTA adjusted to pH 7.2 with CsOH and in the presence of 1 μM glutamate and 1 μM glycine. Single-channel current amplitudes were measured by a semiautomatic procedure by adjusting cursors to baseline and open-channel current amplitudes. The ionic composition of the Cs^+ bath solution was similar to that of the pipette solution. For single-channel blockade experiments, the organic test cation was added to the extracellular or cytoplasmic solution. Reversal potentials of single-channel currents were measured under biionic conditions with the above Cs^+ solution in the bath and a 100 mM test cation solution in the pipette (Villarroel and Sakmann, 1992). Organic cation solutions contained 10 mM histidine adjusted to pH 7.2 with HCl. After current measurement the patch was broken and the potential difference between the open pipette and bath solution was measured. To construct a single-channel current-voltage curve, 1000 or more unitary-current amplitudes were pooled in 2 mV bins and averaged from at least four measurements or more at each potential. A sixth-order polynomial was fitted to interpolate the zero-current potential. The measured open-pipette potential was subtracted from the zero-current potential to obtain the reversal potential.

Reversal potentials were also obtained from ensemble currents in HEK cells and in oocyte outside-out patches. Reversal potentials of whole-cell current in HEK cells were determined at room temperature (20–22°C) in a chamber continuously perfused with rat Ringer's solution (135 mM NaCl, 5.4 mM KCl, 1 mM $MgCl_2$, 1.8 mM $CaCl_2$, 5 mM HEPES, pH 7.2 adjusted with NaOH). The recording pipette solution contained 140 mM CsCl, 10 mM EGTA, 10 mM HEPES, and 1 mM $MgCl_2$, pH 7.2 adjusted with CsOH (23.5 mM of CsOH were necessary to add for the adjustment). The extracellular solutions were applied by a double-barreled piezo-driven application pipette. The control Cs^+ solution contained 140 mM CsCl, 10 μM glycine, and 10 mM HEPES adjusted to pH 7.2 with 3.5 mM CsOH (i.e., nominally Ca^{2+}-free). Test solutions contained the test cation at a concentration of 140 mM and 10 μM glycine. The buffer was 10 mM histidine titrated to pH 7.2 with HCl, except for Tris and Arg solutions, which were directly titrated to pH 7.2 with HCl.

Reversal potentials with oocyte outside-out patches were measured with pipettes containing 100 mM Cs^+, 10 mM HEPES, and 10 mM BAPTA adjusted to pH 7.2 with CsOH (23.5 mM). Extracellular solution contained either 100 mM Cs^+ or the test cation (100 mM), 1 mM $CaCl_2$ and 10 μM glycine. The presence of Ca^{2+} ions in this solution was necessary for stable outside-out patches. For Cs^+ and NH_4^+, the buffer was 10 mM HEPES titrated to pH 7.2 with the corresponding hydroxide. Other organic ion solutions were buffered as above.

Both in HEK cells and outside-out patches from oocytes, agonist was applied for 100–200 ms by using a piezo-driven double-barreled application system (Sommer et al., 1990). One barrel contained the test cation solution and the other contained in addition 100 μM glutamate. Current was measured at the peak of the response at a given membrane potential, which was changed in both ascending and descending sequences at intervals of 2–10 mV. The zero-current potential was measured in Cs^+ solution, then in test cation solution followed by a control in Cs^+ solution. The reversal potential was determined as the zero-current potential in the organic ion solution minus the average of the zero-current potentials measured in Cs^+ solution before and after. The junction potentials between the Cs^+/Ringer's solution interface and test cation/Ringer's solution were determined separately using a pipette filled with 3 M KCl and were used to obtain the reversal potentials. For different test solutions the junction potentials were in the range of 4–6 mV.

Blockade analysis

The reduction of the single-channel current amplitudes in solutions containing, in addition to Cs^+, one of the organic test cation species X was described by a simple blockade model (Woodhull, 1973), which assumes that the block caused by the test cations is very fast and reduces the apparent single-channel current amplitude at our frequency resolution (3 kHz). The current in the presence of a blocking test cation added to the extracellular side of the channel is described by

$$i_x(V) = i_0(V)/(1 + [X]/Kd(V)) \quad (1)$$

$$Kd(V) = Kd(0)e^{(z\delta FV/RT)} \quad (2)$$

where $i_0(V)$ and $i_x(V)$ are single-channel current amplitudes in the absence and presence of a blocker at a concentration [X] and at membrane potential V, respectively. $Kd(0)$ is an apparent dissociation constant at 0 membrane potential and $z\delta$ is the fraction of the electric field that contributes to the energy of the ion at the blocking site. R, T, and F have their usual meaning. The current amplitude at −150 mV for different concentrations of blocking cation was fitted using Eq. 1. At least three different concentrations were used for each blocker. We then used this $Kd(-150)$ value to fit each current-voltage curve to determine $z\delta$ by combining Eq. 1 with the following relation:

$$Kd(V) = Kd(-150)e^{(z\delta F(V+150)/RT)}. \quad (3)$$

Notice that $Kd(-150)\,e^{(z\delta\,F\,(150)/RT)}$ is $Kd(0)$ as in Eq. 2. The use of $Kd(-150)$ was necessary because the blockade was relatively weak. The $z\delta$ values determined at different concentrations of X were then averaged. The $Kd(0)$ values were estimated from Eq. 2 using the average $z\delta$.

To determine the parameters of the model for the blockade from the intracellular side, current amplitudes at +150 mV measured for different concentrations of blocker were used to obtain $Kd(+150)$. The voltage dependence of blockade was estimated by using Eqs. 1–3, in which $z\delta$ was replaced by $-z\delta$, and the fitted $Kd(+150)$ value was used instead.

Permeability ratios

The permeability ratio P_x/P_{Cs} was calculated according to the Goldman-Hodgkin-Katz equation in experiments with HEK cells and inside-out patches from oocytes

$$\frac{P_x}{P_{Cs}} = \frac{[Cs]_i}{[X]_o}\exp\left(\frac{FV_{rev}}{RT}\right) \quad (4)$$

where V_{rev} is the reversal potential, $[X]_o$ and $[Cs]_i$ are the concentrations of the species X and Cs^+, respectively, and P_x/P_{Cs} is the permeability ratio of the organic ion X relative to Cs^+.

Correction for Ca^{2+} permeability

The NMDAR channel is highly permeable to Ca^{2+}; therefore, in outside-out patches, the presence of 1 mM Ca^{2+} in the extracellular solution must be taken into account in the calculation of the organic ion permeability.

Permeability ratios, P_X/P_{Cs} and P_{Ca}/P_{Cs}, are related to the reversal potential through the extended Goldman-Hodgkin-Katz equation (Lewis, 1979):

$$V_{rev} = \frac{RT}{F} \mathrm{Ln}\left\{\frac{[Cs]_o + (P_x/P_{Cs})[X]_o + 4(P'_{Ca}/P_{Cs})[Ca]_o}{[Cs]_i + (P_x/P_{Cs})[X]_i + 4(P'_{Ca}/P_{Cs})[Ca]_i e^{FV_{rev}/RT}}\right\} \quad (5)$$

where V_{rev} is the reversal potential measured in the presence of Ca^{2+}, [X], [Ca], and [Cs] are the concentrations of organic test cation, Ca^{2+} and Cs^+, respectively. The subscripts i and o refer to inside and outside, respectively. P_x/P_{Cs} is the permeability ratio of the organic ion X relative to Cs^+ and P'_{Ca}/P_{Cs} is the calcium permeability (see Lewis, 1979; Iino et al., 1990). In our experimental conditions, Eq. 5 becomes

$$V_{rev} = \frac{RT}{F} \mathrm{Ln}\left\{\frac{(P_x/P_{Cs})[X]_o + 4(P'_{Ca}/P_{Cs}[Ca]_o}{[Cs]_i}\right\}. \quad (6)$$

This can be written as

$$e^{FV_{rev}/RT} = \frac{P_x}{P_{Cs}}\frac{[X]_o}{[Cs]_i} + 4\frac{P_{Ca}}{P_{Cs}}\frac{1}{(1 + e^{FV_{rev}/RT})}\frac{[Ca]_o}{[Cs]_i}. \quad (7)$$

With 1 mM Ca^{2+} in the extracellular solution and using the estimated P_{Ca}/P_{Cs} = 4.57 (see below), the permeability ratio of an organic cation relative to Cs^+ becomes

$$\frac{P_x}{P_{Cs}}\frac{[X]_o}{[Cs]_i} = e^{FV_{rev}/RT} - 18.28\frac{1}{[Cs]_i(1 + e^{FV_{rev}/RT})}. \quad (8)$$

The P_{Ca}/P_{Cs} of 4.57 corresponds to a reversal potential of −54.2 mV measured in HEK cells in biionic conditions with the impermeant cation TMA (140 mM) and 1 mM Ca^{2+} in external solution and 163.5 mM Cs^+ in the intracellular solution.

RESULTS

Block of NMDAR channels by organic cations

Native and recombinant NMDAR channels adopt several conductance substates (Cull-Candy and Usowicz, 1987; Jahr and Stevens, 1987, Stern et al., 1992). In symmetrical Cs^+ (100 mM) solutions, the main open state of the recombinant NR1-NR2A channel was always clearly distinguished, although infrequent substates were present. Fig. 1 *A* shows a continuous record of single-channel currents from an inside-out patch excised from an oocyte previously injected with NR1 and NR2A subunit-specific mRNAs. Channel openings appeared in bursts with a rather noisy, but well defined, open conductance state (Fig. 1 *B*). These currents were observed only when glutamate was added to the pipette solution. When 0.5 mM Mg^{2+} was added to the pipette solution, single-channel currents were interrupted by frequent brief closing events at negative but not at positive potentials as expected for NMDAR single-channel currents (not shown; Ascher and Nowak, 1988). The single-channel *i-V* relation in symmetrical (100 mM) Cs^+ solutions exhibited a slight inward rectification (Fig. 2, *C* and *D*; filled symbols) with a chord conductance of 57.3 ± 0.6 pS (n = 9, mean ± SE) at −100 mV and 46.2 ± 0.3 pS (n = 5) at +100 mV.

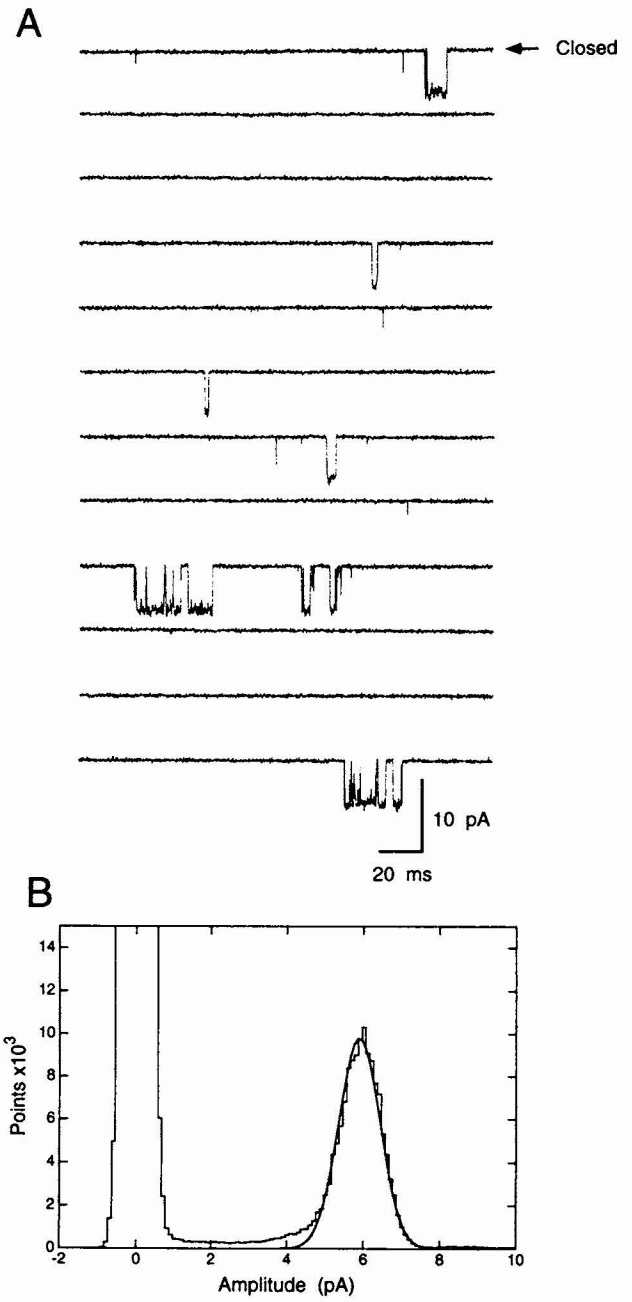

FIGURE 1 Single-channel currents through the recombinant NR1-NR2A channel in *Xenopus* oocyte. (*A*) Continuous record from an inside-out patch isolated from an oocyte injected with the NR1 and NR2A subunit-specific mRNAs. Bath solution (cytoplasmic side) contained 100 mM Cs^+, 10 mM HEPES, and 10 mM EGTA at pH 7.2. Pipette solution (extracellular side) contained in addition 1 μM glutamate and 1 μM glycine. Membrane potential was −100 mV. Inward current is displayed downward. (*B*) Amplitude distribution of current record shown in (*A*). A continuous current record of 3 s in duration was filtered at 3 kHz (−3 dB) and sampled at intervals of 100 μs. Amplitude histogram (0.1 pA bin size) shows a peak near 0 amplitude corresponding to baseline; the smaller peak representing the distribution of open-channel current amplitudes. Smooth curve is fit to a Gaussian function with mean amplitude 5.9 pA and 0.75 pA SD.

Voltage-dependent channel block

Dimensions of an ion conduction pathway may be probed using organic cations of different size that can enter into the channel preventing ion flow in a voltage-dependent way. We examined the blocking action of organic ions with hydrocarbon (TMA, choline, TriEA, TEA, Hme), and polar surfaces (Tris, Arg, NMG) of comparable sizes.

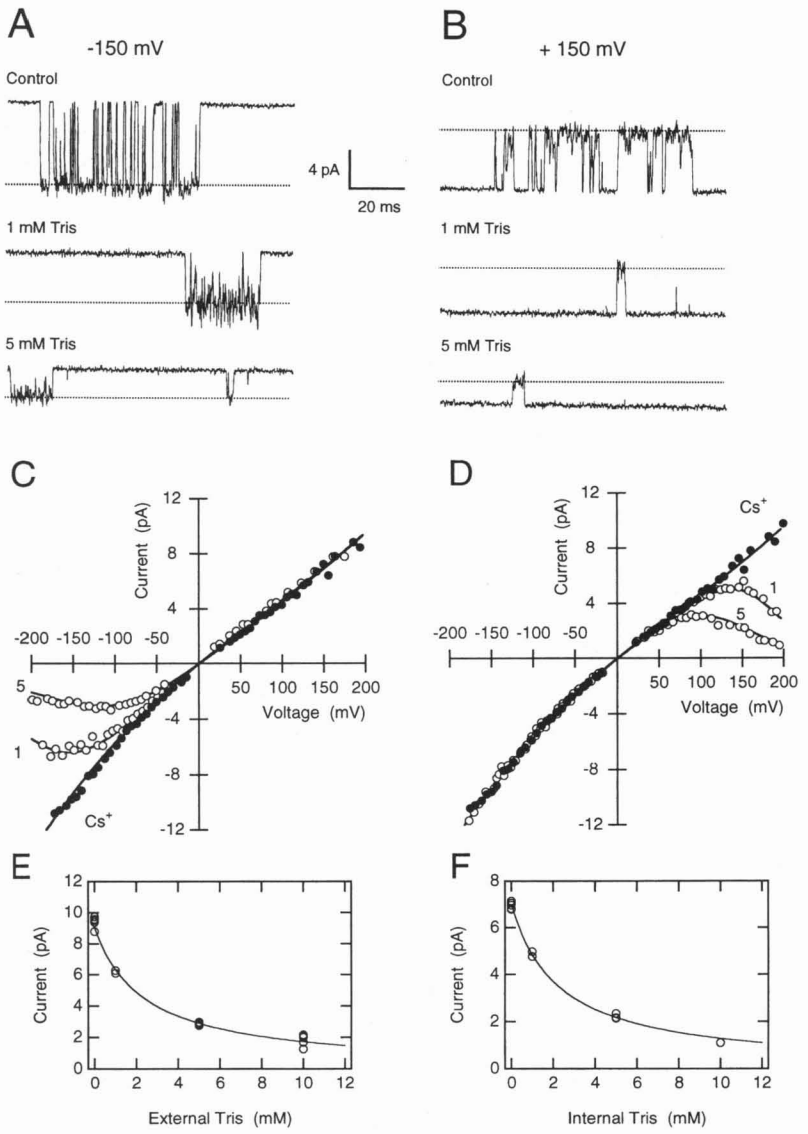

FIGURE 2 Reduction of NR1-NR2A single-channel currents by Tris on the extracellular or cytoplasmic side measured in inside-out patches from *Xenopus* oocytes. (*A*) Single-channel current traces showing reduction in current amplitude caused by external Tris at −150 mV. Filtered at 1 kHz (−3 dB). Notice the increase in noise caused by Tris. Current amplitude was determined by eye as indicated by the dashed lines on the traces. (*B*) Single-channel current traces showing reduction in current amplitude caused by internal Tris at +150 mV, 1 kHz. (*C*) Single-channel *i-V* curves in the absence (●) or presence (○) of 1 and 5 mM Tris in the extracellular (100 mM) Cs^+ solution. Continuous line over the open symbols is the fit to Eq. 2 with $z\delta_o = 0.55$ and $z\delta_o = 0.4$ for 1 and 5 mM, respectively. $Kd(0)_o = 50$ mM. (*D*) Same as (*C*) but with Tris added to the cytoplasmic (100 mM) Cs^+ solution. Filled symbols represent currents in Cs^+ solution without Tris. Fit parameters are $z\delta_i = 0.75$ and $z\delta_i = 0.71$ for 1 and 5 mM, respectively. $Kd(0)_i = 114$ mM. (*E, F*) Concentration dependence of reduction of single-channel currents by extracellular (*E*) or cytoplasmic (*F*) Tris. Open symbols represent currents measured at −150 mV (external Tris) or +150 mV (internal Tris). The continuous line is the best fit to Eq. 1. The $Kd(-150)$ and $Kd(+150)$ were 2.2 and 2.3 mM, respectively.

The blockade by large cations present in the solution facing the extracellular side of the channel will be described first.

Tris added to the extracellular solution reduced Cs^+ inward currents at negative potentials in a concentration- and voltage-dependent fashion with no measurable effect on outward currents (Fig. 2, *A* and *C*). The reduction of inward single-channel current caused by extracellular Tris at −150 mV can be described with an apparent $Kd(-150)$, defined by Eq. 1, of 2.2 mM (Fig. 2, *E*). The fractional electric distance $z\delta_o$ (subscript o corresponds to the blockade from outside) of the blocking site in the open channel reached by external Tris was 0.51 ± 0.07 ($n = 10$), suggesting that extracellular Tris crosses about half of the electric field. Voltage-dependent blocking effects on inward currents were observed with other organic cations that are of comparable or somewhat larger sizes (Table 1). The voltage dependence of the blockade produced by TMA, choline, and TriEA was somewhat smaller (fractional electrical distances of blocking sites were 0.36–0.43) than that of Tris. Hme, which is doubly charged, showed a voltage dependence about twice as large, and Arg, which has two positive and one negative charge, blocked also with a larger voltage dependence (Table 1).

Tris, when added to the cytoplasmic side, reduced outward currents at positive potentials, whereas inward currents were not measurably affected (Fig. 2, *B* and *D*). At +150 mV, the apparent $Kd(150)$ was 2.3 mM (Fig. 2 *F*) with a fractional electrical distance $z\delta_i$ (subscript i corresponds to the blockade from inside) of 0.65 ± 0.17 ($n = 9$). The polar cations (Tris, NMG, and Arg) blocked outward Cs^+ current in a strongly voltage-dependent fashion, whereas TMA, choline, TriEA, Hme, and TEA blocked more weakly and with less voltage dependence, or not at all (Table 1). Thus large organic cations may penetrate into the channel from either the extracellular or the cytoplasmic side indicating the presence of a cavity of at least the size of these ions.

The TEA blockade was more complicated. When added to the extracellular side, it strongly blocked the inward currents

TABLE 1 Blockade parameters of impermeant organic cations

Ion	$Kd(-150)$ mM	$Kd(+150)$ mM	$z\delta_o$	$z\delta_i$	Mean diameter, Å
TMA	4.8	56	0.40 ± 0.02 (3)	0.24 ± 0.08 (9)	5.5
Choline	1.9	11	0.43 ± 0.05 (7)	0.29 ± 0.05 (4)	6.0
TriEA	1.0	*	0.36, 0.37 (2)	*	6.1
Tris	2.2	2.3	0.51 ± 0.07 (10)	0.65 ± 0.17 (9)	5.8
NMG	4.0	17	0.51 ± 0.12 (3)	0.35 ± 0.16 (3)	7.3
Arg	3.8	4.9	0.69 ± 0.04 (5)	0.49 ± 0.12 (4)	6.9
Hme	0.11	*	0.70 ± 0.04 (4)	*	7.1
TEA	0.8	*	0.73 ± 0.12 (7)	*	6.6

$Kd(-150)$ and $Kd(+150)$ refer to apparent dissociation constants calculated using Eq. 1. The $z\delta$ values were obtained for each experiment by fitting *i-V* curves measured with at least three concentrations of blocker. The number of experiments is given in parenthesis. $Kd(0)_o$, the apparent dissociation constant at 0 mV for extracellular cations, was calculated from $Kd(-150)$, which was obtained from the fit to the concentration dependence of the current and the average $z\delta_o$. The values were 53, 24, 50, 239, 85, and 64 mM for TMA, choline, Tris, Arg, NMG, and TEA, respectively. $Kd(0)_i$ was obtained from $Kd(+150)$ and the average $z\delta_i$ for internal blockade. The values were 236, 61, 114, 93, and 139 mM for TMA, choline, Tris, Arg, and NMG, respectively. Both $Kd(0)$ values were calculated using Eq. 3. The mean diameter was calculated as the geometric mean of the dimensions of a box that contains the ion.

*Ions that did not block when added at 5 mM. Blockade parameters not determined.

with an apparent $Kd(-150)$ of 0.8 mM and a $z\delta_o$ of 0.73 ± 0.12 (n = 7), considerably larger than the value expected from the relatively large size of TEA (Table 1), and the absence of multiple charges. On the other hand, internal TEA did not reduce the current. In 10 mM TEA, the conductance at +100 mV was 44.2 ± 0.7 pS (n = 3), not significantly different than that in control conditions. Thus, the blockade caused by TEA differs from that of the other cations of comparable size by a strong voltage dependence and a selective affinity for the extracellular entry of the channel.

Voltage-independent channel blockade

Organic cations smaller than TMA reduced the single-channel conductance but not in a voltage-dependent fashion. TriMA (10 mM) added to the extracellular Cs^+ solution reduced inward currents (37.5 pS mean of 2 at −100 mV), but the block differed from that observed with TMA because the bending of the *i-V* curve at negative potentials was only minor (Fig. 3, *A* and *C*). DMA (10 mM), which is smaller than TriMA, produced a smaller reduction in conductance (45.6 ± 0.7 pS (n = 4) at −100 mV (Fig. 3 *C*)). When these ions were added to the cytoplasmic side the reduction in outward single-channel conductance was even less (43.7 ± 1.5 pS, n = 4 for TriMA (Fig. 3, *B* and *D*) and 40.5 ± 0.6 pS, n = 3 for DMA, not shown).

The reduction of inward and outward single-channel conductance caused by TriMA and DMA resembles that expected for a "permeant-blocking" ion (Dwyer et al., 1980, Sanchez et al., 1986), which transiently binds when passing through the channel. The small reduction in the channel conductance would then be a consequence of the passage of Cs^+ and the less permeant TriMA or DMA ions.

Permeation and transport of organic cations through NMDAR channels

The differences in magnitude and voltage-dependence of the blocking action among organic cations of different sizes suggests that they may block or permeate the channel depending on their size. Ions larger than the narrow portion of the pore block the passage of Cs^+ by steric hindrance and not, for example, by binding to a site common to blocking and permeant ions. This view also suggests that the narrow portion of the NR1-NR2A channel is smaller than a Tris molecule. To estimate the size of the channel constriction, we made reversal potential measurements in biionic conditions with organic test cations on one side of the membrane and Cs^+ on the other.

Permeability measurements

Single-channel currents with Tris as the test cation in inside-out patches (100 mM Tris in the extracellular and 100 mM Cs^+ in the cytoplasmic solution) revealed only outward currents at 0 mV or more positive potentials but no inward currents down to −200 mV (not shown). This could indicate that either Tris is impermeant or the conductance is too small to be detected. Therefore, glutamate-activated ensemble currents were measured from transfected HEK cells and oocyte outside-out patches. In HEK cells outward currents in Tris extracellular solution were observed at potentials as negative as −120 mV (Fig. 4 *A*), and no inward currents were observed even at −150 mV. This result provides an upper limit of <0.01 for the Tris/Cs^+ permeability ratio. Biionic experiments with NMG and Arg also showed that these ions were not measurably permeant because outward currents were observed at −100 mV, and no inward currents at −120 mV. TriEA and Hme were also not measurably permeant. They showed outward currents at potentials as negative as −100 mV, but no detectable inward currents. Experiments with oocyte outside-out patches made in the presence of 1 mM extracellular Ca^{2+} also did not reveal clear inward currents with Tris, TEA, and Arg down to −100 mV.

Permeability differences among ammonium derivatives

The difference in the voltage dependence of channel block between TMA and TriMA (Fig. 3 *C*) suggests that these two ions, which differ in only one methyl group, might behave as impermeant and permeant ions, respectively. In line with this, in biionic experiments with 140 mM TMA on the outside, outward currents could be clearly detected for TMA in HEK cells (n = 7) at membrane potentials negative to −100 mV (Fig. 4 *B*). On the other hand, TriMA showed a clear inward current negative to −60 mV (Fig. 4 *C*) indicating that it is permeant.

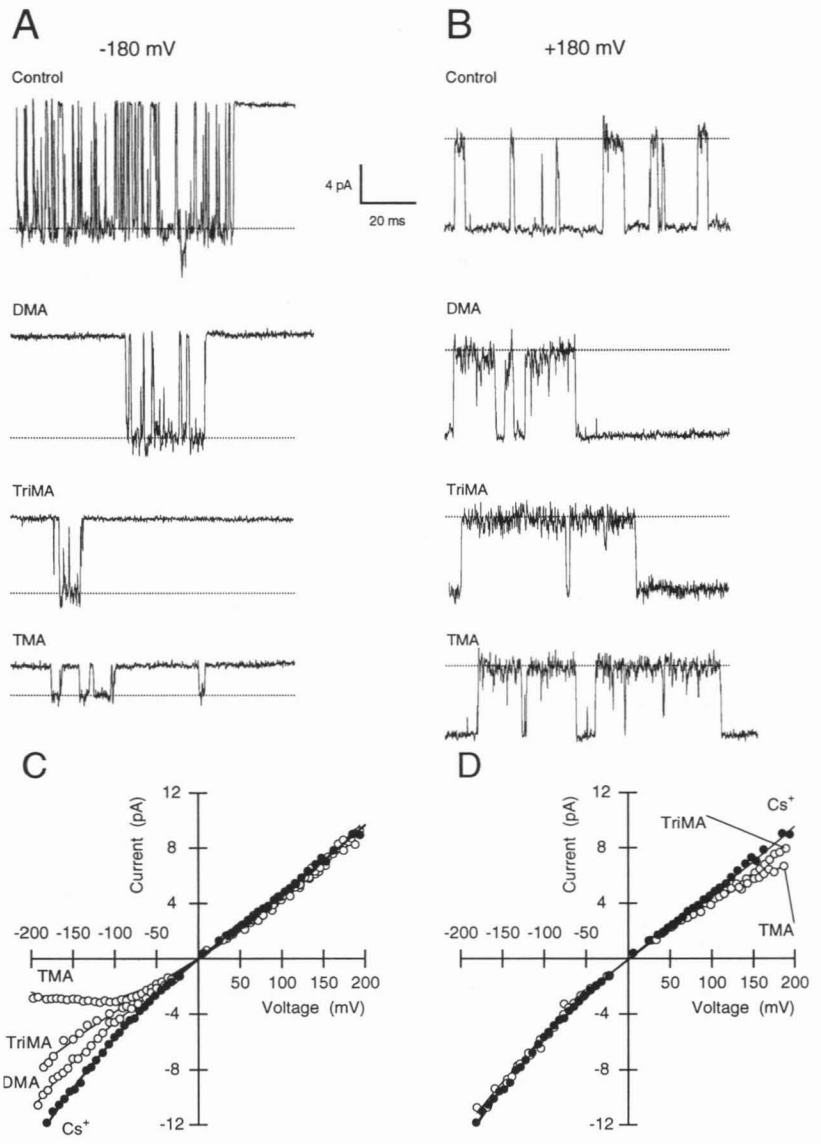

FIGURE 3 Differences in block of the NR1-NR2A channel by NH_4^+ derivatives of different size. (*A*) Single-channel currents measured in inside-out patches of *Xenopus* oocyte in 100 mM symmetrical Cs^+ solution with either 10 mM TMA, TriMA, or DMA added to the external Cs^+ solution. The membrane potential was −180 mV. Filtered at 1 kHz (−3 dB). (*B*) Single-channel current measured in inside-out patches of *Xenopus* oocyte in 100 mM symmetrical Cs^+ solution with either 10 mM TMA, TriMA, or DMA added to the internal Cs^+ solution. The membrane potential was +180 mV, 1 kHz. (*C*) Current-voltage curve measured in inside-out patches of *Xenopus* oocyte in 100 mM symmetrical Cs^+ solution with either 10 mM TMA, TriMA, or DMA added to the external Cs^+ solution. (*D*) Current-voltage curve measured in inside-out patches of *Xenopus* oocyte in 100 mM symmetrical Cs^+ solution with either 10 mM TMA or TriMA added to the internal Cs^+ solution.

The TriMA/Cs^+ reversal potential of whole-cell currents (Fig. 4 *C*) was on average −66.7 ± 2.4 mV (n = 5).

Sieving of permeant organic cations

Several organic cations smaller than TMA were tested and showed that the reversal potential of the NH_4^+ derivatives became less negative as the number of methyl substitutions decreased. In measurements done with NMDARs expressed in HEK cells, the average shift in the reversal potential when external Cs^+ was replaced by DMA (Fig. 4 *D*) was −41.1 ± 4.2 mV (n = 3) and was −20.9 ± 2.7 mV (n = 3) for MA. In single-channel measurements done with NMDARs expressed in oocytes, the reversal potential for NH_4^+ was 4.3 ± 0.9 mV (n = 7), indicating that NH_4^+ is more permeant than Cs^+ (Table 2). Similar permeabilities were calculated for oocyte outside-out patch measurements, corrected for the presence of 1 mM extracellular Ca^{2+} (Fig. 5; Table 2).

Measurements with oocyte inside-out patches in biionic conditions with permeant organic cations (100 mM) in the extracellular solution demonstrated inwardly directed single-channel currents at negative membrane potentials. Chord conductances measured from single-channel current amplitudes at −100 mV decreased as the size of the NH_4^+ derivative increased. The largest conductance 88 ± 3 pS (n = 4) was found for NH_4^+, also the most permeant cation. For MA, DMA, and TriMA, the conductance at −100 mV was 23.7 ± 1.4 pS (n = 4), 9.8 ± 0.5 pS (n = 5), 3.6 ± 1.3 pS (n = 3), respectively.

DISCUSSION

Channel entrances

The recombinant NMDAR channel formed by NR1 and NR2A subunits was blocked by several organic cations in a

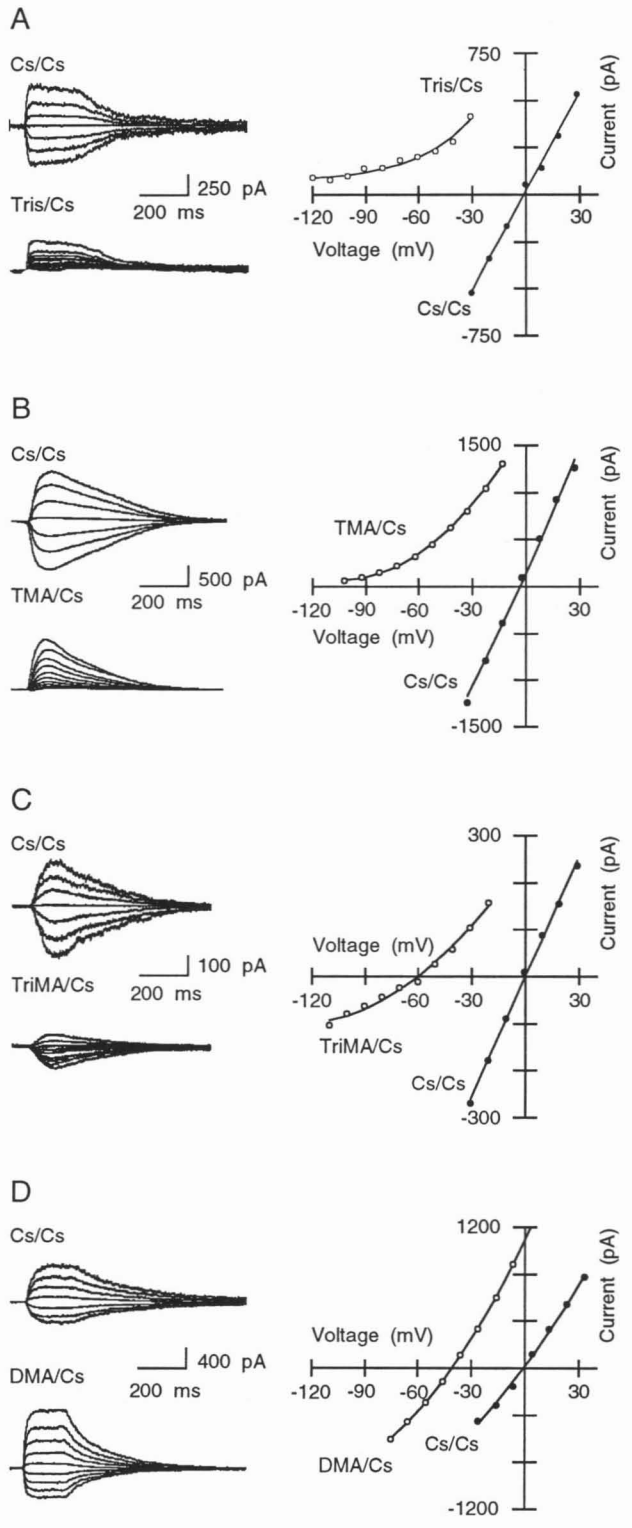

FIGURE 4 Biionic reversal potentials for different organic test cations versus Cs^+ ions determined from whole-cell *I-Vs* of the NR1-NR2A channel expressed in HEK cells. Left panel shows current traces in response to 200-ms (*A* and *D*) or 100-ms (*B* and *C*) pulses of 100 μM glutamate in the presence of 10 μM glycine at several potentials applied to lifted cells bathed either in 140 mM Cs^+ solution or in a solution with Cs^+ replaced by test cations (*A*) Tris; (*B*) TMA; (*C*) TriMA; (*D*) DMA. Inward currents downward, 10 mV voltage intervals. Right panel shows *I-V* curves of peak currents. Continuous line is a fit to a third-order polynomial to interpolate the zero-current potential.

TABLE 2 Permeability ratios P_x/P_{Cs} for organic cations of different sizes

Ion	V_{rev} (mV)	P_x/P_{Cs}	Ion size (Å)
Ammonium	(a) 4.3 ± 0.9 (7)	1.19	3.3 × 3.2 × 3.4
	(b) 5.1 ± 0.1 (3)	1.26	
Hydrazine	(a) −11.4 ± 0.4 (3)	0.95	3.1 × 3.4 × 4.1
MA	(a) −23.1 ± 1.5 (4)	0.5	3.5 × 3.7 × 4.1
	(b) −20.9 ± 2.7 (3)	0.44	
	(c) −13.4, −12.1 (2)	0.49, 0.52	
DMA	(a) −44.9 ± 8.0 (5)	0.21	3.8 × 4.2 × 6.1
	(b) −41.1 ± 4.2 (3)	0.2	
	(c) −28.2 ± 2.7 (3)	0.2	
TriMA	(a) −62.6 ± 3.4 (3)	0.10	4.0 × 5.4 × 6.0
	(b) −66.7 ± 2.4 (5)	0.07	
TMA	(b) <−100 (7)	<0.02	5.5 × 5.5 × 5.5
	(c) <−100 (7)	<0.02	
TriEA	(b) <−100 (3)	<0.02	5.1 × 6.2 × 7.3
Tris	(b) <−120 (4)	<0.01	5.5 × 5.6 × 6.4
	(c) <−120 (3)		
Choline	(b) <−100 (2)	<0.02	5.5 × 5.6 × 7.1
TEA	(b) <−100 (4)	<0.02	5.8 × 7.0 × 7.0
Arg	(b) <−140 (4)	<0.01	4.7 × 6.4 × 11.2
	(c) <−140 (3)		
Hme	(b) <−100 (5)	<0.02	5.5 × 5.5 × 12.0
NMG	(b) <−140 (4)	<0.01	5.0 × 6.4 × 12.0

(a) refers to measurement with inside-out oocyte patches, (b) to whole-cell current measurements with HEK cells, and (c), to outside-out oocyte patch measurements. For (b) and (c), V_{rev} refers to the shift in zero-current potentials when switching from Cs^+ solution to test cation solution (see Materials and Methods). All reversal potentials values (V_{rev}) were corrected for junction potentials. The small asymmetry between $[Cs^+]_o$ and $[Cs^+]_i$ due to the different amount of CsOH added for pH adjustment will produce a Nernst potential difference of $V = 25 \ln([Ca]_o/[Cs]_i)$. This was included in the calculation of the P_x/P_{Cs}. Reversal potentials in outside-out patches (c) were measured in the presence of 1 mM Ca^{2+}; therefore permeability ratios P_x/P_{Cs} were corrected for P_{Ca}/P_{Cs} (see Materials and Methods). Ion sizes correspond to the dimensions of the smallest box that contains the ion as measured with Corey-Pauling-Kolton models (Molecular dimensions of organic ions were kindly provided by Dr. B. Hille, University of Washington).

voltage-dependent way, as if these ions penetrate partially into the electric field across the channel. The calculated apparent dissociation constant for extracellular and intracellular Tris blockade at zero potential (50 mM and 114 mM, respectively) indicated only weak binding of Tris when entering the channel from either side. Similar results for the other impermeant organic cations (legend to Table 1) suggest that organic ions are driven into the pore by voltage rather than by specific interaction with the channel wall. In this sense the blockade mechanism seems to operate partly by steric occlusion.

The voltage dependencies of the block for different ions are different, arguing against a common blocking site (Table 1). The position of the ion along the electric field depends, rather, on its particular geometry and its chemical nature. We classified them accordingly.

Ions with the positive charge surrounded by methyl or ethyl groups (TMA, choline, TriEA) penetrate about 40% of the field (0.36–0.43) from the external side, with the exception of TEA (see below). From the inside the voltage de-

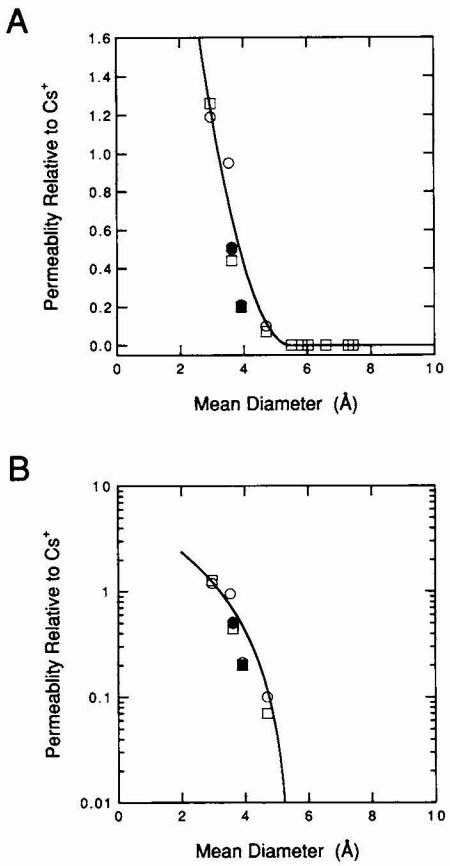

FIGURE 5 Estimates of dimension of the narrow portion of the NR1-NR2A channel. (*A*) Relation between permeability ratio and mean ion size. Relative permeability of organic cations with respect to Cs^+, measured in oocyte inside-out patches (○), oocyte outside-out patches (●), and HEK cells (□), are plotted as a function of the mean diameter of organic cations. Six cations, TMA, Tris, Arg, TEA, choline, and NMG are virtually impermeant ($P_x/P_{Cs} < 0.02$). The continuous line is the best fit to Eq. 9. The parameters were $k = 5.86$ and $d_{pore} = 5.5$ Å. If permeability ratios derived from experiments with 1 mM, extracellular Ca^{2+} were not taken into account for the fit, the estimated d_{pore} varied from 5.4 to 5.7 Å depending on the weighting factor. (*B*) Same as (*A*) with logarithmic *y* axis. This plot includes only "permeant" organic cations, which show a clear reversal potential, *x* axis intercept at 5.5 Å mean diameter.

pendence of the block is smaller or absent. Ions with a more polar surface and the positive charge in one end (Tris and NMG), which are of comparable size, penetrate somewhat more deeply, possibly indicating that —OH groups allow closer interaction with the channel wall. For Tris the sum of the derived electrical distances was somewhat larger than unity. This apparent discrepancy may be understood, at least partly, in terms of the geometry. The positive charge, localized in the ammonium group, could penetrate into the narrow portion of the channel, with the bulky part of the molecule preventing it from passing the channel.

The multiply charged molecules Arg and Hme blocked with a large voltage dependence from the outside, the electrical distance of the blocking site being almost twice that of TMA (Table 1), which is consistent with the idea that two positive charges feel the electric field. For Arg blockade the sum of the two calculated voltage dependencies, like that of Tris, was >1. Arg has three charges, one negative in the carboxyl group, and two positive in the guanidinium and amino group, respectively. The guanidinium group may also penetrate the narrow part of the pore (as indicated by the measurable permeability of hydrazine) with the rest of the molecule occluding the narrow portion of the channel, and giving rise to an apparent crossing in the electrical distances. For the external block the negative charge is left behind in the field resulting in a higher voltage dependence from the outside, as observed in Ca^{2+}-activated K^+ channels (Villarroel et al., 1988).

External TEA blockade exhibited very different behavior in comparison with the other blocking cations, which cannot be understood by steric occlusion alone. TEA is a large symmetrical molecule (see Table 2) with the charge in the center and no polar groups on its surface, and is not expected to penetrate deeper into the pore than, e.g., TriEA. The possibility that more than one TEA molecule occupies the extracellular vestibule, each one contributing partly to the voltage dependence, is also unlikely given that the affinity of TEA for the channel is as weak as that of the other cations (see Table 1 legend). It could be speculated that TEA has a voltage-dependent action on channel gating that could mimic a blocking effect. Alteration of channel gating induced by TEA has been described in native NMDARs (Wright et al., 1991; Koshelev and Khodorov, 1992).

The simplified picture that emerges from the block experiments is that of a channel with a narrow portion preventing the passage of large organic ions. The access to the narrow part is wide enough to accommodate an NMG ion with a calculated mean diameter of 7.3 Å (Table 1) and suggests that the channel contains wider funnels (40 $Å^2$ cross-sectional area) at the extracellular and cytoplasmic entrances leading to the narrower constriction. In addition, the weaker blockade by cations with hydrocarbon surfaces suggest a polar inner face of the pore, in particular for the internal side.

Channel constriction

All molecules larger than TMA, both polar (choline, Tris, Arg, N-methyl-glucamine) and hydrophobic (TEA, Hme), were found to be impermeant in the experimental range of voltages. The narrow constriction of the pore seems to be wide enough to permit passage of TriMA but not of TMA, which is only slightly larger. This difference allows an estimate of the narrow cross section to be made based on geometrical considerations. The cross section of the narrow part, defined as the two smaller dimensions of a box that contains an ion, is 4.0 × 5.4 Å for TriMA and 5.5 × 5.5 Å for TMA. The channel constriction should then have a minimal dimension of 4.0 × 5.4 Å and cross-sectional area on the order of 22 $Å^2$.

An alternative estimate of the dimensions of the narrow portion is obtained by relating the decrease in relative permeability with the increase in ion size for the NH_4^+ methyl

derivatives. A simple hydrodynamic model (Dwyer et al., 1980) assumes that the channel constriction is represented as a water-filled cylinder and that permeability is proportional to the cross-sectional area available for ions ("excluded volume effect"). For a given pore diameter (d_{pore}) the permeability for an ion, relative to Cs^+, is given by

$$P = k(1 - (d_{ion}/d_{pore}))^2 \quad (9)$$

where d_{ion} is derived as above from space-filling molecular models, and k is a proportionality constant. The relationship between reversal potentials and ion sizes is shown in Fig. 5, *A* and *B*. The continuous line is the best fit to Eq. 9 with d_{pore} = 5.5 Å. This estimate of the pore dimension would correspond to a real pore diameter if permeant ions were spheres and the pore would be a cylinder with a cross-sectional area of 24 Å^2.

Comparison with other ion channels

The estimated pore size of 5.5 Å in diameter of the NR1-NR2A channel is markedly smaller than the value previously estimated for native NMDAR channels (Vyklicky et al., 1988; Wright et al., 1991). Recently, a preliminary report describes an NMDAR from CA1 hippocampal neurones with a cross-sectional area of 24 Å^2 (Zarei and Dani, 1993). The pore size of the NMDAR is also smaller than the values obtained for other cation-selective ligand-gated ion channels, which vary between 7.0 and 7.6 Å. AChR channels have a constriction with an estimated mean diameter of 7.0 Å in frog muscle (Dwyer et al., 1980; Huang et al., 1978) and 7.4 Å for recombinant AChR channels (*Torpedo electroplax*, Wang and Imoto, 1992). 5-HT_3-R channels in neuroblastoma cells also have a relatively wide pore of 7.6 Å in diameter (Yakel et al., 1990; Yang, 1990). Anion-selective γ-aminobutyric acid and glycine receptors of mouse spinal cord neurones form channels comparable in size to the NR1-NR2A receptor with an estimated mean diameter of 5.2–5.4 Å (Bormann et al., 1987).

The pore of the NR1-NR2A receptor is slightly smaller than that of a voltage-gated Ca^{2+}-selective channel in frog muscle. There, TMA is a permeant ion suggesting a circular pore of 6 Å in diameter (McCleskey and Almers, 1985).

Channel constriction and molecular structure

Subunits that form ligand-gated ion channels are thought to belong to a superfamily of homologous proteins (Unwin, 1989; Betz, 1990). This view is mainly based on similarities in the hydropathy profiles of their predicted amino acid sequences, in particular, the prediction of four transmembrane segments M1–M4 and TM1–TM4. So far, there is little structural information for ligand-gated ion channels other than for the AChR channel from *Torpedo* electric organ (Unwin, 1993), which is asymmetrical and characterized by large extracellular and cytoplasmic funnels bordering the narrow portion. The constriction is formed, presumably, by the M2 segments of the constituting subunits. The NR1-NR2A channel described here differs from recombinant AChR channels in its smaller cross-sectional area of the narrow portion (22–24 Å^2 vs. ~40 Å^2).

Point mutational analysis of recombinant NMDAR channels has shown asparagine residues in the TM2 segments, which are thought to be homologous to the M2 segment of the AChR and are critical for Ca^{2+} permeability and Mg^{2+} block (Burnashev et al., 1992; Mori et al., 1992), suggesting that in NMDAR channels the TM2 segments also contribute to the pore formation. It remains to be investigated whether those amino acids of the TM2 segment that form the blocking site for Mg^{2+} and the selectivity filter for Ca^{2+}, or the adjacent amino acids, also contribute to the formation of the channel constriction.

We thank Mr. T. Kuner for oocyte injection and Ms. S. Grünewald for cell culture and transfections, and Drs. L. Wollmuth and K. Imoto for helpful discussions and critical reading of the manuscript. We are also grateful to Prof. B. Hille (Department of Physiology and Biophysics, University of Washington) for providing molecular dimensions for organic ions, and Prof. P. Seeburg (Center for Molecular Biology, University of Heidelberg) for providing clones of the NMDA NR1 and NR2A subunits. The expert secretarial assistance of Ms. G. Dücker and Ms. H. Spiegel is also acknowledged.

REFERENCES

Ascher, P, and L. Nowak. 1988. The role of divalent cations in the N-methyl-D-aspartate responses of mouse central neurones in culture. *J. Physiol.* 399:247–266.

Armstrong, C. M. 1975. Potassium pores of nerve and muscle membranes. *In* Membranes, Vol. 3. G. Eisenmann, editor. Marcel Dekker, Inc., New York. 325–580.

Betz, H. 1990. Homology and analogy in transmembrane channel design: lessons from synaptic membrane proteins. *Biochemistry.* 29:3591–3599.

Bormann, J., O. P. Hamill, and B. Sakmann. 1987. Mechanism of anion permeation through channels gated by glycine and gamma-amino butyric acid in mouse cultured spinal neurones. *J. Physiol.* 385:243–286.

Burnashev, N., R. Schoepfer, H. Monyer, J. P. Ruppersberg, W. Günther, P. H. Seeburg, and B. Sakmann. 1992. Control by asparagine residues of calcium permeability and magnesium blockade in the NMDA receptor. *Science.* 257:1415–1419.

Chen, C., and H. Okayama. 1987. High-efficiency transformation of mammalian cells by plasmid DNA. *Mol. Cell. Biol.* 7:2745–2752.

Coronado, R., and C. Miller. 1982. Conduction and block by organic cations in a K^+-selective channel from sarcoplasmic reticulum incorporated into planar phospholipid bilayers. *J. Gen. Physiol.* 79:529–547.

Cull-Candy. S., and M. M. Usowicz. 1987. Multiple-conductance channels activated by excitatory amino acids in cerebellar neurons. *Nature (Lond.).* 325:525–528.

Cull-Candy. S., J. R. Howe, and D. C. Ogden. 1988. Noise and single channels activated by excitatory amino acids in rat cerebellar granule neurones. *J. Physiol.* 400:189–222.

Dwyer, T. M., D. J. Adams, and B. Hille. 1980. The permeability of the endplate channel to organic cations in frog muscle. *J. Gen. Physiol.* 75: 469–492.

Hamill, O. P., A. Marty, E. Neher, B. Sakmann, and F. J. Sigworth. 1981. Improved patch-clamp techniques for high-resolution current recording from cells and cell-free membrane patches. *Pflügers Arch.* 391:85–100.

Hille, B. 1992. Ionic Channels of Excitable Membranes. Sinauer Associates Inc., Sunderland, Mass.

Huang, L. Y., W. A. Catterall, and G. Ehrenstein. 1978. Selectivity of cations and nonelectrolytes for acetylcholine-activated channels in cultured muscle cells. *J. Gen. Physiol.* 71:397–410.

Iino, N., S. Ozawa, K. Tzuzuki. 1990. Permeation of calcium through excitatory amino acid receptor channels in cultured rat hippocampal neurones. *J. Physiol.* 424:151–165.

Ishii, T., K. Moriyoshi, H. Sugihara, K. Sakurada, H. Kadotani, M. Yokoi, C. Akazawa, R. Shigemoto, N. Mizuno, M. Masu, and S. Nakanishi. 1993. Molecular characterization of the family of the N-methyl-D-aspartate receptor subunits. *J. Biol. Chem.* 268:2836–2843.

Jahr, C. E., and C. F. Stevens. 1987. Glutamate activates multiple single channel conductances in hippocampal neurons. *Nature (Lond).* 325: 522–525.

Koshelev, S., and B. Khodorov. 1992. Tetraethylammonium and tetrabutylammonium as tools to study NMDA channels of neuronal membrane. *Biol. Membr.* 9:1064–1068 (in Russian).

Kutsuwada, T., N. Kashiwabuchi, H. Mori, K. Sakimura, E. Kushiya, K. Araki, H. Meguro, H. Masaki, T. Kumanishi, M. Arakawa, and M. Mishina. 1992. Molecular diversity of the NMDA receptor channel. *Nature (Lond.).* 358:36–41.

Lewis, C. 1979. Ion-concentration dependence of the reversal potential and the single channel conductance of ion channels at the frog neuromuscular junction. *J. Physiol.* 286:417–445.

Mayer, M. L., and G. L. Westbrook. 1984. Mixed-agonist action of excitatory amino acids on mouse spinal cord neurones under voltage clamp. *J. Physiol.* 354:29–53.

McCleskey, E. W., and W. Almers. 1985. The Ca channel in skeletal muscle is a large pore. *Proc. Natl. Acad. Sci. USA.* 82:7149–7153.

Methfessel, C., V. Witzemann, T. Takahashi, M. Mishina, S. Numa, and B. Sakmann. 1986. Patch clamp measurements on *Xenopus laevis* oocytes: currents through endogenous channels and implanted acetylcholine receptor and sodium channels. *Pflügers Arch.* 407:577–588.

Miller, C. 1982. Bis-quaternary ammonium blockers as structural probes of the sarcoplasmic reticulum K^+ channel. *J. Gen. Physiol.* 79:869–891.

Monyer, H., N. Burnashev, D. J. Laurie, B. Sakmann, and P. H. Seeburg. 1994. Development and regional expression in the rat brain and functional properties of four NMDA receptors. *Neuron.* 12:529–540.

Monyer, H., R. Sprengel, R. Schoepfer, A. Herb, M. Higuchi, H. Lomeli, N. Burnashev, B. Sakmann, and P. H. Seeburg. 1992. Heteromeric NMDA receptors: molecular and functional distinction of subtypes. *Science.* 256:1217–1221.

Mori, H, H. Masaki, T. Yamakura, and M. Mishina. 1992. Identification by mutagenesis of a Mg^{2+}-block site of the NMDA receptor channel. *Nature (Lond.).* 358:673–675.

Moriyoshi, K., M. Masu, T. Ishii, R. Shigemoto, N. Mizuno, and S. Nakanishi. 1991. Molecular cloning and characterization of the rat NMDA receptor. *Nature (Lond.).* 354:31–37.

Sanchez, J. A., J. A. Dani, D. Siemen, and B. Hille. 1986. Slow permeation of organic cations in acetylcholine receptor channels *J. Gen. Physiol.* 87:985–1001.

Sommer, B., K. Keinänen, T. A. Verdoon, W. Wisden, N. Burnashev, A. Herb, M. Köhler, T. Takagi, B. Sakmann, and P. H. Seeburg. 1990. Flip and flop: A cell-specific functional switch in glutamate operated channels of the CNS. *Science.* 249:1580–1585.

Stern, P., P. Behe, R. Schoepfer, and D. Colquhoun. 1992. Single-channel conductances of NMDA receptors expressed from cloned cDNAs: comparison with native receptors. *Proc. R. Soc. Lond. Ser. B. Biol. Sci.* 250: 271–277.

Stern, P., M. Cik, D. Colquhoun, and F. A. Stephenson. 1994. Single channel properties of cloned NMDA receptors in a human cell line: comparison with results from *Xenopus* oocytes. *J. Physiol.* 476:391–397.

Unwin, N. 1989. The structure of ion channels in membranes of excitable cells. *Neuron.* 3:665–676.

Unwin, N. 1993. Nicotinic acetylcholine receptor at 9 Å resolution. *J. Mol. Biol.* 229:1101–1124.

Villarroel, A. 1993. Probing the NMDA receptor channel pore with organic ions. *Biophys. J.* 64:115a.

Villarroel, A., O. Alvarez, A. Oberhauser, and R. Latorre. 1988. Probing a Ca^{2+}-activated K^+ channel with quaternary ammonium ions. *Pflügers Arch.* 413:118–126.

Villarroel, A., and B. Sakmann. 1992. Threonine in the selectivity filter of the acetylcholine receptor channel. *Biophys. J.* 62:196–205.

Vyklicky, L. J., J. Krusek, and C. Edwards. 1988. Differences in the pore sizes of the N-methyl-D-aspartate and kainate cation channels. *Neurosci. Lett.* 89:313–318.

Wang, F., and K. Imoto. 1992. Pore size and negative charge as structural determinants of permeability in the Torpedo nicotinic acetylcholine receptor channel. *Proc. R. Soc. Lond. Ser. B. Biol. Sci.* 250:11–17.

Watkins, J. C. 1981. Pharmacology of excitatory amino acid receptors. *In* Glutamate Transmitter in the Central Nervous System. P. J. Roberts, J. Storm-Mathisen, and G. A. R. Johnston, editors. Wiley and Sons, New York. 1–24.

Woodhull, A. M. 1973. Ionic blockage of sodium channels in nerve. *J. Gen. Physiol.* 61:687–708.

Wright, J. M., P. A. Kline, and L. M. Nowak. 1991. Multiple effects of tetraethylammonium on N-methyl-D-aspartate receptor-channels in mouse brain neurons in cell culture. *J. Physiol.* 439:579–604.

Yakel, J. L., X. M. Shao, and M. B. Jackson. 1990. The selectivity of the channel coupled to the $5\text{-}HT_3$ receptor. *Brain Res.* 533:46–52.

Yang, J. 1990. Ion permeation through 5-hydroxytryptamine-gated channels in neuroblastoma N18 cells. *J. Gen. Physiol.* 96:1177–1198.

Zarei, M. M., and J. A. Dani. 1993. Structural and permeability properties of the N-methyl-D-aspartate receptor channel. *Abstr. Soc. Neurosci.* 19, I:278.